Perfect plane-wave source for a high-order symplectic finite-difference time-domain scheme*

Wang Hui(王 辉)[a], Huang Zhi-Xiang(黄志祥)[a]†, Wu Xian-Liang(吴先良)[a,b], and Ren Xin-Gang(任信钢)[a]

[a] *Key Laboratory of Intelligent Computing & Signal Processing of Ministry of Education, Anhui University, Hefei* 230039, *China*
[b] *Department of Physics and Electronic Engineering, Hefei Normal University, Hefei* 230061, *China*

(Received 31 March 2011; revised manuscript received 9 May 2011)

The method of splitting a plane-wave finite-difference time-domain (SP-FDTD) algorithm is presented for the initiation of plane-wave source in the total-field / scattered-field (TF/SF) formulation of high-order symplectic finite-difference time-domain (SFDTD) scheme for the first time. By splitting the fields on one-dimensional grid and using the nature of numerical plane-wave in finite-difference time-domain (FDTD), the identical dispersion relation can be obtained and proved between the one-dimensional and three-dimensional grids. An efficient plane-wave source is simulated on one-dimensional grid and a perfect match can be achieved for a plane-wave propagating at any angle forming an integer grid cell ratio. Numerical simulations show that the method is valid for SFDTD and the residual field in SF region is shrinked down to −300 dB.

Keywords: splitting plane-wave finite-difference time-domain, high-order symplectic finite-difference time-domain scheme, plane-wave source

PACS: 47.11.Bc **DOI:** 10.1088/1674-1056/20/11/114701

1. Introduction

The finite-difference time-domain method is one of the most convenient tools for solving electromagnetic field problems.[1,2] In the finite-difference time-domain (FDTD), plane-wave sources are often used for a variety of simulations where the scattered field is of interest. For the efficient simulation of a plane-wave, the total-field/scattered-field (TF/SF) formulation as outlined in Ref. [3] is such a well-developed and popular method for introducing arbitrary incident fields into FDTD. Based on the equivalence principle, the whole computational domain is divided into two regions: a TF region where both incident and scattered fields reside, and an SF region where only the scattered fields exist. Therefore, in theory, the fields in the SF region are identically zero when no scatters exist in the TF region. Incident field in the TF region can be introduced simply by applying a tangential source field to the boundary between the two regions, which is often called the Huygens' surface. The Huygens' surface works by adjusting the value of nodes adjacent to the boundary, i.e., nodes whose neighbouring nodes lie on the other side of the boundary.

Although this formulation is advantageous, in practice, the TF/SF formulation suffers field leakage in the SF region in the case of oblique incident plane-wave. A lot of work in reducing the leakage error has been done in the past decade.

To accomplish the TF/SF formulation, a computationally efficient one-dimensional (1D) auxiliary propagator called the incident field array (IFA)[3,4] is often used to propagate a plane-wave source concurrent with the main simulation domain in time domain, which is used as a lookup table to populate the Huygens' surface. Unfortunately, because of interpolation and dispersion mismatches between the 1D propagator and two-dimensional (2D)/three-dimensional (3D) main grids, the incident field always leaks into the SF region to disturb the scattered field. Improvement on the IFA has been made by researchers, if the correction technique of either Ref. [5] or Ref. [6] is employed, the leakage error can be suppressed by almost −70 dB.

In frequency domain, the analytic field propagator (AFP) method[7] where the discrete Fourier transform-based wave injection is utilized, improves the error dramatically (−180 dB). However, one of its primary drawbacks is its demand of vast computa-

*Project supported by the National Natural Science Foundation of China (Grant Nos. 60931002 and 61101064) and the Universities Natural Science Foundation of Anhui Province, China (Grant Nos. KJ2011A002 and 1108085J01).

†Corresponding author. E-mail: zxhuang@ahu.edu.cn

© 2011 Chinese Physical Society and IOP Publishing Ltd

tional resources. In addition, 1D multipoint auxiliary source propagator[8] describes an efficient perfectly matched FDTD plane-wave source in time domain derived directly from the wave equation for 2D problems with −300 dB of leakage error. A versatile split-field 1D propagator[9] in which Maxwell's equations in their split-field form are used, also achieves machine level field isolation, but it is still in 2D implementations. It is noticeable that Tan and Potter[10] reported on an optimized AFP (O-AFP) technique which extends its applicability to 3D and FDTD-DPW (FDTD discrete planewave)[11] that is fully implemented in 3D simulations and extends its applicability to non-standard FDTD methods, both of which maintain the accuracy (−300 dB).

The other problems with FDTD are its demand of vast computational resources, and the significant accumulated errors from numerical instability and dispersion. Fortunately, new schemes which are named the symplectic schemes[12,13] are widely studied because of their great advantages in recent years. For overcoming the shortcomings of the FDTD mentioned above, the symplectic FDTD (SFDTD) scheme[14] and its improved schemes[15,16] are proposed, owing to its higher stability, lower dispersion and nondissipation. When this scheme is used for practical applications such as radar cross-section (RCS) determination, near or far field scattering, etc., it is of vital importance to illuminate the objects by a plane-wave. However, how to apply a perfect plane-wave source to SFDTD scheme in 3D, especially to high-order SFDTD scheme, is still an unsolved problem.

In what follows, we provide the details of how the SP-FDTD technique can be adjusted to make the technique practical for the application to high-order SFDTD scheme in 3D problems and its feasibility is confirmed by the nature of numerical plane-wave in FDTD.

2. Background information

2.1. Nature of numerical plane-wave in FDTD

Let $\boldsymbol{p} = (p_x, p_y, p_z) = (\sin\theta\cos\varphi, \sin\theta\sin\varphi, \cos\theta)$ be a unit vector defining the normal direction of a planar wavefront, with θ and φ being the polar and the azimuthal angles, respectively. The electric field for a plane-wave propagating along the $\boldsymbol{p}$ direction is of the form $\boldsymbol{E}(r,t)$ and the magnetic field is in the form of $\boldsymbol{H}(r,t)$ on 1D grid, where the scalar r is measured along a line parallel to $\boldsymbol{p}$ and $r = \boldsymbol{p}\cdot\boldsymbol{x} = p_x x + p_y y + p_z z$ with $\boldsymbol{x} = (x, y, z)$.

The fields in discrete FDTD grids exist at locations defined by $\boldsymbol{X}_{\rm d} = (i_x\Delta x, i_y\Delta y, i_z\Delta z)$, with i_x, i_y and i_z being integers, likewise, $r_{\rm d} = p_x i_x\Delta x + p_y i_y\Delta y + p_z i_z\Delta z$. Let $g(r_{\rm d}, t)$ and $g(\boldsymbol{X}_{\rm d}, t)$ denote field components in discrete spaces R^1 and R^3, respectively. In order to have equivalent plane-waves in both spaces, it is required that $\partial_\xi g(\boldsymbol{X}_{\rm d}, t) = \partial_\xi r_{\rm d}\partial r_{\rm d} g(r_{\rm d}, t)$, $\xi = x$, y or z. As stated in Ref. [11], it is expressed as

$$\frac{g(\boldsymbol{X}_{\rm d} + \frac{\Delta\xi}{2}, t) - g(\boldsymbol{X}_{\rm d} - \frac{\Delta\xi}{2}, t)}{\Delta\xi} = \frac{g(r_{\rm d} + \frac{p_\xi\Delta\xi}{2}, t) - g(r_{\rm d} - \frac{p_\xi\Delta\xi}{2}, t)}{\Delta\xi}. \quad (1)$$

Here, we concentrate on the fourth-order space difference scheme, such as

$$\partial_\xi g(\boldsymbol{X}_{\rm d}, t) = \frac{9}{8}\cdot\frac{g(\boldsymbol{X}_{\rm d} + \frac{\Delta\xi}{2}, t) - g(\boldsymbol{X}_{\rm d} - \frac{\Delta\xi}{2}, t)}{\Delta\xi} - \frac{g(\boldsymbol{X}_{\rm d} + \frac{3\Delta\xi}{2}, t) - g(\boldsymbol{X}_{\rm d} - \frac{3\Delta\xi}{2}, t)}{24\Delta\xi}, \quad (2a)$$

thus according to Eq. (1), we have

$$\partial_\xi g\,(\boldsymbol{X}_{\rm d}, t) = \frac{9}{8}\cdot\frac{g(i_r\Delta r + \frac{m_\xi\Delta r}{2}, t) - g(i_r\Delta r - \frac{m_\xi\Delta r}{2}, t)}{\Delta\xi} - \frac{g(i_r\Delta r + \frac{3m_\xi\Delta r}{2}, t) - g(i_r\Delta r - \frac{3m_\xi\Delta r}{2}, t)}{24\Delta\xi}, \quad (2b)$$

where $r_{\rm d} = i_r\Delta r$, i_r is an integer and

$$p_\xi\Delta\xi = m_\xi\Delta r. \quad (3)$$

Equation (3) is the rational angle condition[8,9] which restricts the plane-wave to the propagation at an angle determined by $\tan\varphi = m_y\Delta x/m_x\Delta y$ and $\tan\theta = \sqrt{m_x^2/\Delta x^2 + m_y^2/\Delta y^2}/(m_z/\Delta z)$.

2.2. Review of SFDTD scheme

The Maxwell's equations in an isotropic, lossless and sourceless medium can be rewritten as

$$\partial_t\begin{pmatrix}\boldsymbol{H}(\boldsymbol{x},t)\\ \boldsymbol{E}(\boldsymbol{x},t)\end{pmatrix} = (\boldsymbol{P}+\boldsymbol{Q})\begin{pmatrix}\boldsymbol{H}(\boldsymbol{x},t)\\ \boldsymbol{E}(\boldsymbol{x},t)\end{pmatrix}, \quad (4)$$

where

$$\boldsymbol{P}=\begin{pmatrix}\{0\} & -\boldsymbol{R}/\mu\\ \{0\} & \{0\}\end{pmatrix},\quad \boldsymbol{Q}=\begin{pmatrix}\{0\} & \{0\}\\ \boldsymbol{R}/\varepsilon & \{0\}\end{pmatrix}, \tag{5}$$

in which $\{0\}$ is the 3×3 null matrix and $\boldsymbol{R}$ is the 3D curl operator in Ref. [16].

Since the matrices $\boldsymbol{P}$ and $\boldsymbol{Q}$ do not commute, the symplectic integrator is applicable to Maxwell's equations. The solution of the electromagnetic field during the time-step Δt can be exactly expressed by the exponential operator $\mathrm{e}^{\Delta t(\boldsymbol{P}+\boldsymbol{Q})}$. Using the product of elementary symplectic mapping, the operator is approximated as[14−16]

$$\mathrm{e}^{\Delta t(\boldsymbol{P}+\boldsymbol{Q})}=\prod_{l=1}^{m}\mathrm{e}^{D_l\Delta t\boldsymbol{Q}}\,\mathrm{e}^{C_l\Delta t\boldsymbol{P}}+O\left(\Delta t^{w+1}\right), \tag{6}$$

where C_l and D_l are constant coefficients of the propagator and w is the order of the approximation. Accordingly, the m stage and wth-order SFDTD scheme is constructed. Note that, in this paper, the five-stage fourth-order SFDTD scheme has been used. The relevant coefficients under the condition of the time-reversible constraint are the same as those in Ref. [16].

The expressions of the update equations about field components at the l-stage can be expressed as

$$\boldsymbol{H}^{n+l/5}=\boldsymbol{H}^{n+(l-1)/5}-\frac{C_l\Delta t}{\mu}\cdot\boldsymbol{R}\times\boldsymbol{E}^{n+(l-1)/5}, \tag{7a}$$

$$\boldsymbol{E}^{n+l/5}=\boldsymbol{E}^{n+(l-1)/5}+\frac{D_l\Delta t}{\varepsilon}\cdot\boldsymbol{R}\times\boldsymbol{H}^{n+l/5}. \tag{7b}$$

For example, the further expression of the electric field E_z at the second stage is as follows:

$$\begin{aligned}E_z^{n+2/5}\Big(i,j,k+\frac{1}{2}\Big)=&E_z^{n+1/5}\Big(i,j,k+\frac{1}{2}\Big)+\frac{D_2\Delta t}{\varepsilon\Delta x}\times\left\{\frac{1}{8}\left[9H_y^{n+2/5}\Big(i+\frac{1}{2},j,k+\frac{1}{2}\Big)-9H_y^{n+2/5}\Big(i-\frac{1}{2},j,k+\frac{1}{2}\Big)\right]\right.\\&\left.-\frac{1}{24}\left[H_y^{n+2/5}\Big(i+\frac{3}{2},j,k+\frac{1}{2}\Big)-H_y^{n+2/5}\Big(i-\frac{3}{2},j,k+\frac{1}{2}\Big)\right]\right\}\\&-\frac{D_2\Delta t}{\varepsilon\Delta y}\times\left\{\frac{1}{8}\left[9H_x^{n+2/5}\Big(i,j+\frac{1}{2},k+\frac{1}{2}\Big)-9H_x^{n+2/5}\Big(i,j-\frac{1}{2},k+\frac{1}{2}\Big)\right]\right.\\&\left.-\frac{1}{24}\left[H_x^{n+2/5}\Big(i,j+\frac{3}{2},k+\frac{1}{2}\Big)-H_x^{n+2/5}\Big(i,j-\frac{3}{2},k+\frac{1}{2}\Big)\right]\right\}.\end{aligned} \tag{8}$$

According to Eqs. 2(a), 2(b) and (3), Eq. (8) takes a new form

$$\begin{aligned}E_z^{n+2/5}\Big(i_r+\frac{m_z}{2}\Big)=&E_z^{n+1/5}\Big(i_r+\frac{m_z}{2}\Big)+\frac{D_2\Delta t}{\varepsilon\Delta x}\times\left\{\frac{1}{8}\left[9H_y^{n+2/5}\Big(i_r+\frac{m_x+m_z}{2}\Big)-9H_y^{n+2/5}\Big(i_r-\frac{m_x-m_z}{2}\Big)\right]\right.\\&\left.-\frac{1}{24}\left[H_y^{n+2/5}(i_r+\frac{3m_x+m_z}{2})-H_y^{n+2/5}\Big(i_r-\frac{3m_x-m_z}{2}\Big)\right]\right\}\\&-\frac{D_2\Delta t}{\varepsilon\Delta y}\times\left\{\frac{1}{8}\left[9H_x^{n+2/5}\Big(i_r+\frac{m_y+m_z}{2}\Big)-9H_x^{n+2/5}\Big(i_r-\frac{m_y-m_z}{2}\Big)\right]\right.\\&\left.-\frac{1}{24}\left[H_x^{n+2/5}\Big(i_r+\frac{3m_y+m_z}{2}\Big)-H_x^{n+2/5}\Big(i_r-\frac{3m_y-m_z}{2}\Big)\right]\right\}.\end{aligned} \tag{9}$$

A plane-wave in FDTD is anisotropic because each propagation direction $\boldsymbol{p}$ has a unique dispersion relation. Specifically, the dispersion relation of the five-stage fourth-order SFDTD scheme is given in Ref. [14] as

$$\left(\sin\frac{\omega\Delta t}{2}\right)^2+\frac{1}{4}\sum_{p=1}^{5}g_p\left[-\frac{1}{\mu\varepsilon}\Delta t^2\left(\eta_x^2+\eta_y^2+\eta_z^2\right)\right]^p=0, \tag{10}$$

where

$$g_p=\sum_{1\le i_1\le j_1<i_2\le j_2<\cdots<i_p\le j_p\le 5}C_{i_1}D_{j_1}C_{i_2}D_{j_2}\cdots C_{i_p}D_{j_p}+\sum_{1\le i_1<j_1\le i_2<j_2\le\cdots\le i_p<j_p\le 5}D_{i_1}C_{j_1}D_{i_2}C_{j_2}\cdots D_{i_p}C_{j_p}, \tag{11}$$

$$\eta_\xi = \frac{27(\mathrm{e}^{\frac{-j\bar{k}_\xi\Delta\xi}{2}} - \mathrm{e}^{\frac{j\bar{k}_\xi\Delta\xi}{2}}) - (\mathrm{e}^{\frac{-3j\bar{k}_\xi\Delta\xi}{2}} - \mathrm{e}^{\frac{3j\bar{k}_\xi\Delta\xi}{2}})}{-24j\Delta\xi}, \tag{12}$$

with $\bar{k}_\xi(\xi = x, y, z)$ being the component of the numerical wavenumber.

3. Formulation

Considering that the subspace r is a linear function of $\boldsymbol{x}$, Maxwell's equations for the incident plane-wave can be expressed as

$$\partial_t \begin{pmatrix} \boldsymbol{H}^{\mathrm{inc}}(r,t) \\ \boldsymbol{E}^{\mathrm{inc}}(r,t) \end{pmatrix} = \begin{pmatrix} 0 & \frac{1}{\mu}\partial_r \\ \frac{1}{\varepsilon}\partial_r & 0 \end{pmatrix} \begin{pmatrix} \boldsymbol{H}^{\mathrm{inc}}(r,t) \\ \boldsymbol{E}^{\mathrm{inc}}(r,t) \end{pmatrix}. \tag{13}$$

The incident fields $\boldsymbol{H}^{\mathrm{inc}}(r,t)$ and $\boldsymbol{E}^{\mathrm{inc}}(r,t)$ on 1D grid are split, respectively, into

$$\boldsymbol{H}^{\mathrm{inc}}(r,t) = \boldsymbol{e}_x \boldsymbol{H}_x^{\mathrm{inc}}(r,t) + \boldsymbol{e}_y H_y^{\mathrm{inc}}(r,t) + \boldsymbol{e}_z H_z^{\mathrm{inc}}(r,t), \tag{14a}$$

$$\boldsymbol{E}^{\mathrm{inc}}(r,t) = \boldsymbol{e}_x E_x^{\mathrm{inc}}(r,t) + \boldsymbol{e}_y E_y^{\mathrm{inc}}(r,t) + \boldsymbol{e}_z E_z^{\mathrm{inc}}(r,t). \tag{14b}$$

As shown in Fig. 1, the auxiliary 1D grid of the proposed scheme uses a uniform Δr spacing specified by Eq. (3) and the electromagnetic fields on 1D grid are staggered and the distance between the co-located electric field and the co-located magnetic field is $\Delta r/2$. As a result, each field component in 3D grids has a value available directly from the 1D grid, for example, $\boldsymbol{E}^{\mathrm{inc}}(\boldsymbol{X}_{\mathrm{d}}, t) = \boldsymbol{E}^{\mathrm{inc}}(r_{\mathrm{d}}, t)$. Furthermore, m_ξ is restricted to odd integers[9] and any choice other than $m_x = m_y = m_z = 1$ means more than one node on 1D grid needs to be enforced correctly for the hard source initiation (see Ref. [9] for explanation in detail).

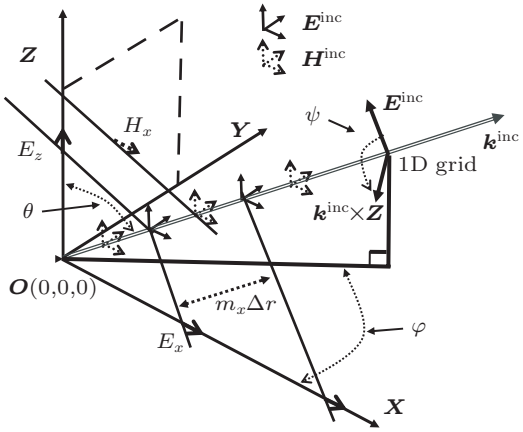


Fig. 1. Perspective view of the fields in main 3D grids, and the field splitting on 1D grid with $m_x = 1$. The projection of the field on the 1D grid is also shown. The orientation angle ψ for $\boldsymbol{E}^{\mathrm{inc}}$ relative to the incident-wave polarization is specified.

Utilizing the relationship and the invariance in both spaces, Eq. (13) can be indicated as

$$\partial_t \begin{pmatrix} \boldsymbol{H}^{\mathrm{inc}}(r,t) \\ \boldsymbol{E}^{\mathrm{inc}}(r,t) \end{pmatrix} = (\boldsymbol{P} + \boldsymbol{Q}) \begin{pmatrix} \boldsymbol{H}^{\mathrm{inc}}(r,t) \\ \boldsymbol{E}^{\mathrm{inc}}(r,t) \end{pmatrix}. \tag{15}$$

Similarly, the expressions of the 1D incident plane-wave are obtained for a 5-stage and 4-order SFDTD scheme as

$$\boldsymbol{H}^{\mathrm{inc},n+\frac{l}{5}} = \boldsymbol{H}^{\mathrm{inc},n+\frac{(l-1)}{5}} - \frac{C_l\Delta t}{\mu}\cdot\boldsymbol{R}\times\boldsymbol{E}^{\mathrm{inc},n+\frac{(l-1)}{5}}, \tag{16a}$$

$$\boldsymbol{E}^{\mathrm{inc},n+\frac{l}{5}} = \boldsymbol{E}^{\mathrm{inc},n+\frac{(l-1)}{5}} + \frac{D_l\Delta t}{\varepsilon}\cdot\boldsymbol{R}\times\boldsymbol{H}^{\mathrm{inc},n+\frac{l}{5}}. \tag{16b}$$

In view of

$$\partial_\xi g(r_{\mathrm{d}}, t) = \frac{g(r_{\mathrm{d}} + p_\xi\Delta\xi/2) - g(r_{\mathrm{d}} - p_\xi\Delta\xi/2)}{\Delta\xi}, \tag{17}$$

the detailed expressions of the incident fields can be obtained, for example, the update equation of the incident electric field $E_z^{\mathrm{inc}}(r,t)$ at the second stage can be expressed as

$$\begin{aligned} E_z^{\mathrm{inc},n+2/5}\Big(i_r + \frac{m_z}{2}\Big) &= E_z^{\mathrm{inc},n+1/5}\Big(i_r + \frac{m_z}{2}\Big) \\ &+ \frac{D_2\Delta t}{\varepsilon\Delta x}\left\{\frac{1}{8}\left[9H_y^{\mathrm{inc},n+2/5}\Big(i_r + \frac{m_x+m_z}{2}\Big) - 9H_y^{\mathrm{inc},n+2/5}\Big(i_r - \frac{m_x-m_z}{2}\Big)\right]\right. \\ &\left. - \frac{1}{24}\left[H_y^{\mathrm{inc},n+2/5}(i_r + \frac{3m_x+m_z}{2}) - H_y^{\mathrm{inc},n+2/5}\Big(i_r - \frac{3m_x-m_z}{2}\Big)\right]\right\} \\ &- \frac{D_2\Delta t}{\varepsilon\Delta y}\left\{\frac{1}{8}\left[9H_x^{\mathrm{inc},n+2/5}\Big(i_r + \frac{m_y+m_z}{2}\Big) - 9H_x^{\mathrm{inc},n+2/5}\Big(i_r - \frac{m_y-m_z}{2}\Big)\right]\right. \\ &\left. - \frac{1}{24}\left[H_x^{\mathrm{inc},n+2/5}\Big(i_r + \frac{3m_y+m_z}{2}\Big) - H_x^{\mathrm{inc},n+2/5}\Big(i_r - \frac{3m_y-m_z}{2}\Big)\right]\right\}. \end{aligned} \tag{18}$$

Note that update equations for the other fields components (E_x, E_y, H_x, H_y, H_z) are also necessary. The update equation (18) on 1D grid has the same form as the update equation (9) on 3D grids, so do the update equations for other fields components in both spaces. Therefore, the plane-waves simulated by both sets of update equations and the corresponding dispersion relations are the same.

In order to construct a projection operator, the anisotropy is considered, which is needed for hard-wiring the initial 1D grid nodes.[9] Letting

$$D_\xi = \sqrt{-\sum_{p=1}^{m} g_p \left(-\frac{\Delta t^2 \eta_\xi^2}{\mu\varepsilon}\right)^p}, \tag{19}$$

the associated FDTD polarization angles $\bar{\varphi}$ and $\bar{\theta}$ should be derived from the dispersion relation and given by

$$\tan\bar{\varphi} = D_y/D_x, \tan\bar{\theta} = \sqrt{D_x^2 + D_y^2}/D_z. \tag{20}$$

It should be noted that our method presented here can be directly extended to the standard high-order FDTD(S24) and the standard FDTD algorithm by letting $m = 1$ and $g_1 = 1.0$.

4. Numerical validation

In this section, to validate the performance of the proposed method for the high-order SFDTD scheme, two numerical examples are presented. The same simulated parameters are used for both examples as follows. The size of computational domain is $120\Delta \times 60\Delta \times 60\Delta$ ($\Delta x = \Delta y = \Delta z = \Delta$) with PEC around the computational domain. The TF region measures $100\Delta \times 40\Delta \times 40\Delta$ surrounded by an additional 10Δ of SF region on each side. In order to measure the leakage error in the SF region, the background is selected as free space without scatters in the TF region. For minimizing the numerical errors, the magnetic field is normalized by wave impedance of free space and the source E^{inc} is renormalized to its maximum value. The incident plane-wave is designed with $m_x = 3$, $m_y = 5$, $m_z = 7$ ($\varphi \approx 59.03°$, $\theta \approx 39.79°$) and polarization angle $\psi = 20°$.

In the first example, a sine wave source $s(t) = \sin(2\pi f_0 t)$ is used with $f_0 = 4.5$ GHz. The simulation is performed 400 time steps ($n_{\max} = 400$) with $\Delta t \approx 3.33 \times 10^{-12}$ s and the spatial discretization $\Delta \approx 3.3$ mm. Cross-sectional plots of the electric field E_y in the xz-plane and the magnetic field H_y in the xy-plane are provided in Fig. 2, and it is evident from the figure that there is no field leaking into the SF region.

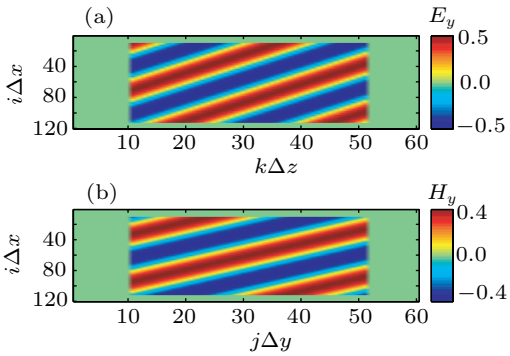


Fig. 2. (colour online) Distributions of electric field E_y in the xz-plane (a) and magnetic field H_y in the xy-plane (b) for 400 time steps with sine wave source.

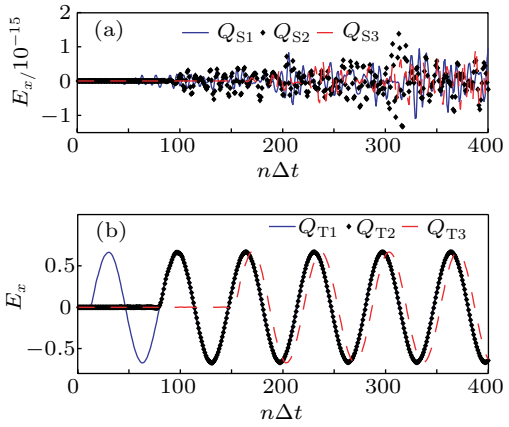


Fig. 3. (colour online) Electric field E_x values at Q_{S1}, Q_{S2} and Q_{S3} in the SF region (a), and electric field E_x values at Q_{T1}, Q_{T2} and Q_{T3} in the TF region (b). $n_{\max} = 400$.

The leakage errors can be measured by examining the scattered field in the SF region due to no scatterer in the TF region. The values of electric field E_x at six measuring points are recorded. There are three measuring points in the SF region (subscript S) at $Q_{S1} = (8\Delta, 8\Delta, 8\Delta)$, $Q_{S2} = (60\Delta, 20\Delta, 8\Delta)$ and $Q_{S3} = (112\Delta, 20\Delta, 20\Delta)$, one near the source and two further away, as well as three measuring points in the TF region (subscript T) at $Q_{T1} = (12\Delta, 12\Delta, 12\Delta)$, $Q_{T2} = (60\Delta, 20\Delta, 12\Delta)$ and $Q_{T3} = (108\Delta, 20\Delta, 20\Delta)$ to demonstrate the level of accuracy of the incident field. As shown in Fig. 3(b), the curves for the incident electric field E_x in the TF region plotted by Q_{T1}, Q_{T2} and Q_{T3} clearly show that those fields are delayed with respect to each other but with small phase error. Furthermore, because of several boundary points that are hard-sourced to initiate the wave on 1D grid, the beginning of the waveform has a small distortion but it turns quite well later. The exciting result is that the fields in the SF region are 15 orders of magnitude smaller than those in the TF region (around −300 dB). As shown in Fig. 2 and Fig. 3(b), the signal seems to

have undergone significant attenuation when propagating through the computational domain due to the incident-wave polarization.

The second example is to investigate the property of the method over a wide frequency band. We consider a frequency modulated gaussian pulse traveling on 1D grid. The time waveform of the pulse is described as

$$s(t) = \sin(2\pi f_0 t)\ \mathrm{e}^{-4\pi\left(\frac{t-t_0}{\tau}\right)^2}$$

with $f_0 = 1$ GHz, $\tau = 2 \times 10^{-9}$ s and $t_0 = 6 \times 10^{-9}$ s. Figure 4 shows the intensities of the electric field E_x against time for Q_{T1} and Q_{T3} and the leakage errors of Q_{S1} and Q_{S3} in the SF region, respectively. The simulation is run for 900 time steps with $\Delta = 1.5$ cm and $\Delta t = 1.5 \times 10^{-11}$ s. The maximum leakage errors of Q_{S1} and Q_{S3} are about -302.4 dB and -306.7 dB respectively. Similar leakage errors have also been obtained when they are tested in a larger range of angles with different sources. Therefore, -300 dB incident field isolation error is obtained.

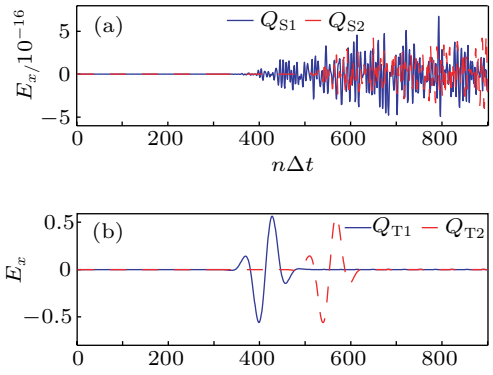


Fig. 4. (colour online) Electric field E_x values at Q_{S1} and Q_{S3} in the SF region (a), and electric field E_x values at Q_{T1} and Q_{T3} in the TF region (b). $n_{\max} = 900$.

5. Conclusions

The use of the SP-FDTD for the excitation of plane-wave is presented for a high-order SFDTD scheme. By studying the nature of the numerical plane-wave in FDTD, the rationality and feasibility of the method are discussed and proved. The method can achieve the perfect dispersion matching between 1D grid and 3D grids, and numerical results show that the method holds true for both single frequency and a wide frequency band with -300 dB of leakage error.

References

[1] Wang S Y, Liu S B and Li L W J 2010 *Chin. Phys.* B **19** 084101

[2] Ding L, Liu J S and Wang K J 2010 *Chin. Phys.* B **19** 127302

[3] Taflove A and Hagness S C 2005 *Computational Electrodynamics: The Finite-Difference Time-Domain Method* (3 edn.) (Norwood, MA: Artech House) pp. 186–210

[4] Winton S C, Kosmas P and Rappaport C M 2005 *IEEE Trans. Antennas Propag.* **53** 1721

[5] Guiffaut C and Mahdjoubi K 2000 *IEEE Antennas Propag. Soc. Int. Symp.*, Salt Lake City, UT, **1** 236

[6] Oguz U and Gurel L 1998 *IEEE Trans. Micro. Theory Tech.* **46** 869

[7] Schneider J B 2004 *IEEE Trans. Antennas Propag.* **52** 3280

[8] Tan T and Potter M 2007 *IEEE Antennas Wireless Propag. Lett.* **6** 144

[9] Hadi F 2009 *IEEE Trans. Antenna Prop.* **57** 2691

[10] Tan T and Potter M 2010 *IEEE Trans. Antenna Prop.* **58** 824

[11] Tan T and Potter M 2010 *IEEE Trans. Antenna Prop.* **58** 2641

[12] Zhang C L, Qi Y Y, Liu X S and Ding P Z 2009 *Acta Phys. Sin.* **58** 3078 (in Chinese)

[13] Liu S X, Guo Y X and Liu C 2008 *Acta Phys. Sin.* **57** 1311 (in Chinese)

[14] Hirono T, Lui W, Seki S and Yoshikuni Y 2001 *IEEE Trans. Microw. Theory Tech.* **49** 1640

[15] Sha W, Huang Z X, Chen M S and Wu X L 2008 *IEEE Trans. Antennas Propag.* **56** 493

[16] Wang J Y, Liu P and Long Y L 2010 *IEEE Antennas and Wireless Propag. Lett.* **9** 371